

Path to Wigner localization in circular quantum dots

Lang Zeng,¹ W. Geist,¹ W. Y. Ruan,¹ C. J. Umrigar,² and M. Y. Chou¹

¹*School of Physics, Georgia Institute of Technology, Atlanta, Georgia 30332-0430, USA*

²*Laboratory of Atomic and Solid State Physics, Cornell University, Ithaca, New York 14853, USA*

(Received 3 March 2009; revised manuscript received 13 May 2009; published 26 June 2009)

Accurate multideterminant ground-state energies of circular quantum dots containing $N \leq 13$ electrons as a function of interaction strength have been evaluated by the diffusion quantum Monte Carlo method. Two unique features are found for these confined two-dimensional systems: (1) as the electron density decreases, the quantum dots favor states with zero orbital angular momentum ($L=0$); and (2) for some values of N , the ground state cannot be fully spin-polarized because of a symmetry constraint.

DOI: [10.1103/PhysRevB.79.235334](https://doi.org/10.1103/PhysRevB.79.235334)

PACS number(s): 73.21.La, 02.70.Ss, 73.63.Kv

I. INTRODUCTION

Circular quantum dots containing a finite number of electrons can be created in two-dimensional (2D) semiconductor structures. They behave like artificial “atoms” with physical properties tunable by adjusting system parameters.^{1–4} By changing the confining potential, the electron density can be varied so that the system can continuously transform between a weakly interacting regime (high density) and a strongly interaction one (low density). Therefore, these quantum dots offer a unique opportunity to study the fundamental physics of many-electron interactions in a controllable fashion.

Due to the Coulomb interaction and electron correlation, Wigner crystallization⁵ in quantum dots occurs in two limiting situations: in systems subjected to a strong magnetic field and in systems with a low electron density. In the former case, all electrons condense into the lowest Landau level, facilitating analytical and numerical studies. The rich physics in the evolution from a Fermi liquid to a Wigner lattice (including the connection with fractional quantum Hall effect, the composite fermion approach, and the rotating Wigner molecule picture) has been extensively investigated and largely understood.^{6–12} For quantum dots with a low electron density, however, numerical simulations are indispensable and computationally quite challenging. Existing studies reached different conclusions regarding various possible transitions that take place as the electron density (effective interaction strength) decreases (increases).^{5,11–18} By examining the electron density and pair density, recent diffusion quantum Monte Carlo calculations^{18,19} have provided information on “incipient” Wigner localization in the intermediate density region. It is found that the one-particle density develops sharp rings as the electron density decreases, while the pair density shows both radial and angular inhomogeneity.^{18,19} Our current study aims to sort out these intermediate ground states and their characteristics as a function of interaction strength in order to understand the fundamentally important correlation effect in a 2D confined system.

In atomic physics, the ground state of a multielectron open-shell atom can be determined by Hund’s rules, which capture the correct physics in an interacting electronic system: by maximizing the total spin S and, for a given spin the

total angular momentum L of valence electrons, the electron-electron interaction energy can be effectively minimized. These rules may not hold for 2D circular quantum dots. In this paper, we report a diffusion quantum Monte Carlo study of electron correlation in the quantum dots for various confinement strengths and electron numbers. Our results show that the conventional Hund’s rules need to be modified as the interaction strength increases, and in these N -electron artificial atoms, the total angular momentum L tends to be minimized to zero, as the system evolves toward a Wigner state in the absence of an external magnetic field. We also find that for some values of N , a fully spin-polarized and Wigner-localized ground state is forbidden by symmetry, and that the critical density parameter r_c for the transition to a fully polarized ground state is highly N dependent.

II. CALCULATIONAL DETAILS

The model system we consider has N electrons moving in two spatial dimensions and laterally confined by a parabolic potential $m^* \omega^2 r^2 / 2$, where m^* is the electron effective mass, r the radius, and ω the strength of the confining potential. When energy is scaled by $\hbar \omega$ and length scaled by the oscillator length $\ell_0 = (\hbar / m^* \omega)^{1/2}$, the Hamiltonian is

$$H = \frac{1}{2} \sum_{i=1}^N (-\nabla_i^2 + r_i^2) + \lambda \sum_{i>j}^N \frac{1}{r_{ij}}, \quad (1)$$

where \mathbf{r}_i is the displacement of the i th electron from the center of the quantum dot and r_{ij} is the separation of an electron pair. $\lambda \equiv \ell_0 / a_B$, where a_B is the effective Bohr radius for the host semiconductor, is a dimensionless system parameter proportional to $1/\sqrt{\omega}$. A large λ implies weak confinement, low-electron density, and strong effective interaction. The magnitude of λ determines the dynamical properties of the system under investigation.

The numerical methods employed in this work are similar to those in Ref. 18, but more Slater determinants (SDs) are incorporated in order to ensure the numerical accuracy. The calculation comprises the following four steps: (1) Kohn-Sham local-density approximation (LDA) orbitals are used to construct Slater determinants. (2) Configuration state functions (CSFs), i.e., linear combinations of determinants that are eigenstates of \hat{L}^2 , \hat{S}^2 , and \hat{S}_z are constructed. (3) The trial

TABLE I. Comparison of DMC energies (see text) of states $[L, S]=[0, 1]$ and $[2, 2]$ with those obtained by exact diagonalization (ED) for $N=4$ (Ref. 22). Energies are in effective Hartree $H^* = m^* e^4 / (\hbar^2 \epsilon^2)$. The numbers in parentheses are statistical errors in the last digit.

N_{det}	λ	DMC ₀	DMC ₂	DMC ₄	ED
		1	20	152	24358
[0,1]	2	3.40241(7)	3.40150(6)	3.40087(5)	3.40450
	4	1.19004(2)	1.18949(2)	1.18925(2)	1.18952
	6	0.65584(1)	0.65551(1)	0.655431(7)	0.655439
	8	0.432553(8)	0.432377(6)	0.432338(5)	0.432338
	10	0.314243(6)	0.314145(5)	0.314134(4)	0.314120
	15	0.176972(4)	0.176950(3)	0.176947(2)	0.176961
	20	0.118291(5)	0.118268(1)	0.118266(1)	0.118501
N_{det}		1	15	82	8721
[2,2]	2	3.56311(3)	3.56296(2)	3.56289(2)	3.56338
	4	1.20984(1)	1.20970(1)	1.20971(1)	1.20978
	6	0.66124(1)	0.66117(1)	0.661176(5)	0.661181
	8	0.434746(5)	0.434692(4)	0.434689(4)	0.434692
	10	0.315349(4)	0.315330(4)	0.315325(3)	0.315323
	15	0.177351(4)	0.177325(4)	0.177317(1)	0.177320
	20	0.118471(6)	0.118440(1)	0.1184368(6)	0.118503

wave function consists of the product of a linear combination of CSFs and the Jastrow factor. The CSF and Jastrow coefficients are optimized to minimize the variational energy. (4) The resulting optimized trial wave function is used to compute the diffusion Monte Carlo (DMC) energy²⁰ within the fixed-node approximation. The increased accuracy attained by using multi-CSF wave functions and by optimizing the coefficients of the determinants in conjunction with the Jastrow parameters is crucial in identifying the physics discussed in this work.²¹ In some cases we included states with up to four intershell excitations, but found that for $\lambda \leq 10$ and $N \leq 13$, a truncation of the Hilbert space by ignoring the SDs with more than two intershell excitations would not change the conclusions drawn in the following discussion. We have also studied a few quantum dots with $\lambda > 10$, where LDA orbitals are difficult to generate, so the Fock-Darwin one-particle states are used.

III. RESULTS AND DISCUSSIONS

In order to demonstrate the accuracy attained, we compare in Table I the DMC energies for a $N=4$ dot obtained with single determinant, and multiple determinant wave functions, obtained by exciting either two or four electrons from the dominant determinant, with exact diagonalization results.²² We note that in most cases the quadruple excitation DMC energies are more accurate (lower) than the exact diagonalization energies, even though the number of determinants employed is far smaller.

In Table II we show the electronic configurations of the ground states for quantum dots with 3–13 electrons in the

small- λ regime (weak interaction, $\lambda \approx 1.9$). The many-body states are specified by the total angular momentum L and total spin S , and the single-particle orbitals by the principal quantum number n and angular momentum l . For noninteracting particles in a 2D harmonic potential, the single-particle states are Fock-Darwin orbitals with energy $(2n+|l|+1)\hbar\omega$. States with the same value of $2n+|l|$ are degenerate, e.g., $(n, l) = (0, \pm 2)$ and $(1, 0)$. With interaction, the

TABLE II. Ground-state electronic configurations for 2D circular quantum dots with $N=3-13$ electrons for interaction strength $\lambda \approx 1.9$. The one-particle states are represented by the principal quantum number n and angular momentum l . L and S are the total angular momentum and spin, respectively.

n	0	0	0	1	0	1	L	S
l	0	± 1	± 2	0	± 3	± 1		
$N=3$	$\uparrow\downarrow$	\uparrow					1	1/2
4	$\uparrow\downarrow$	$\uparrow\uparrow$					0	1
5	$\uparrow\downarrow$	$\uparrow\downarrow\uparrow$					1	1/2
6	$\uparrow\downarrow$	$\uparrow\downarrow\uparrow\downarrow$					0	0
7	$\uparrow\downarrow$	$\uparrow\downarrow\uparrow\downarrow$	\uparrow				2	1/2
8	$\uparrow\downarrow$	$\uparrow\downarrow\uparrow\downarrow$	$\uparrow\uparrow$				0	1
9	$\uparrow\downarrow$	$\uparrow\downarrow\uparrow\downarrow$	$\uparrow\uparrow$	\uparrow			0	3/2
10	$\uparrow\downarrow$	$\uparrow\downarrow\uparrow\downarrow$	$\uparrow\downarrow\uparrow\downarrow$				0	0
	$\uparrow\downarrow$	$\uparrow\downarrow\uparrow\downarrow$	$\uparrow\downarrow\uparrow$	\uparrow			2	1
11	$\uparrow\downarrow$	$\uparrow\downarrow\uparrow\downarrow$	$\uparrow\downarrow\uparrow\downarrow$	\uparrow			0	1/2
12	$\uparrow\downarrow$	$\uparrow\downarrow\uparrow\downarrow$	$\uparrow\downarrow\uparrow\downarrow$	$\uparrow\downarrow$			0	0
13	$\uparrow\downarrow$	$\uparrow\downarrow\uparrow\downarrow$	$\uparrow\downarrow\uparrow\downarrow$	$\uparrow\downarrow$	\uparrow		3	1/2

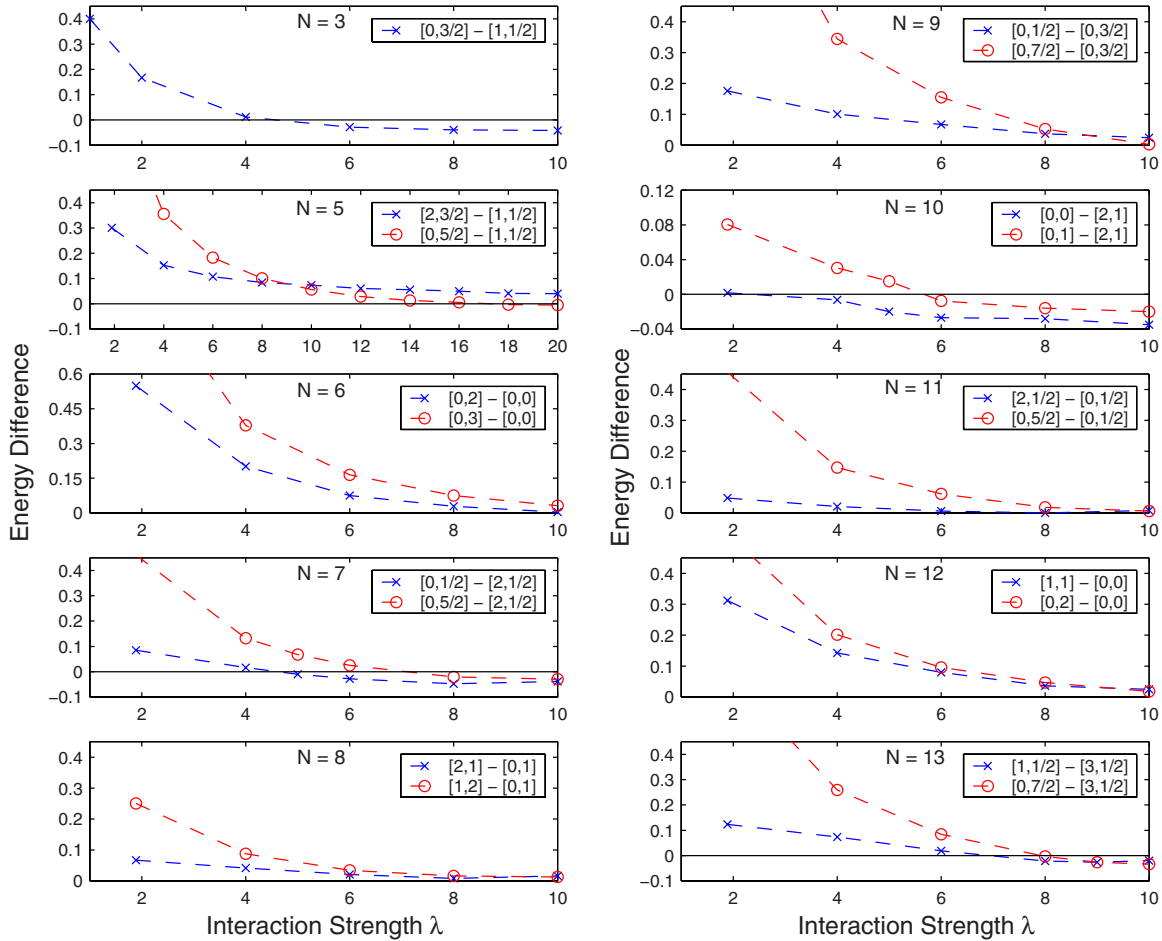


FIG. 1. (Color online) Energy differences between low-lying states $[L,S]$ and the ground state listed in Table II for $N=3$, and 5–13. Energies are in $\hbar\omega$, with ω being the strength of the confining potential.

selfconsistent potential lowers the states with the larger l , e.g., $(0, \pm 2)$ and $(1,0)$ states become two subshells with a small energy gap, so do $(0, \pm 3)$ and $(1, \pm 1)$.

For a specified filling of the subshells, analogously to the case of real atoms, Hund’s first rule specifies that the state with maximal spin, S , will be the ground state. Maximal spin polarization keeps the electrons apart so that the electron-electron interaction energy can be lowered for a given average distance of the electrons from the center of the dot. This allows the electrons to move closer to the center of the dot and lower the total potential energy, although the electron-electron interaction energy is higher. For $N=9$, the promotion energy across the small gap between $(n,l)=(0, \pm 2)$ and $(1,0)$ states is more than compensated by the gain in the exchange energy. For $N=10$, one electron can be promoted from the $(0, \pm 2)$ subshell to the $(1,0)$ subshell to create a $[L,S]=[2,1]$ state, which turns out to be indistinguishable in energy with the state $[0,0]$ at $\lambda \approx 1.9$. For the N values in Table II the symmetries of the many-body ground states, $[L,S]$ are uniquely determined by the electronic configuration (subshell filling) for $N=3,5,6,7,11,12,13$, whereas, Hund’s first rule needs to be invoked to specify the symmetries for $N=4,8,9,10$. Although Hund’s second rule is not explicitly invoked here, as will be shown below, when the interaction strength increases, the total angular momentum L

does play an important role in determining the ground state of the quantum dot, in such a way that the trend is to minimize L .

In Fig. 1 we present the energy differences between a few low-lying states and the ground states in Table II as a function of the dimensionless interaction strength λ for $N=3$ and $N=5-13$. ($N=4$ is not shown because $[0,1]$ continues to be the ground state up to $\lambda \approx 15$.) We focus on λ values from 2 to 10, which is the region for “incipient” Wigner crystallization.¹⁸ Calculations of many different states are first performed at $\lambda=10$, and only the states with low energies are kept for further studies at other λ values as shown in Fig. 1. (Even though these low-lying states at $\lambda=10$ are close in energy, we still have an energy difference of at least 5–10 error bars to distinguish them.)

The transition patterns in Fig. 1 for $N \leq 13$ exhibit some unexpected trends for the range of λ we have studied. Ground-state transitions are seen for $N=3, 5, 7, 10$, and 13 , for which the reference ground state at $\lambda \approx 1.9$ has a nonzero L . When a transition takes place, the new ground states take a lower angular momentum L' ($L'=0$ for $N=3, 5, 7$, and 10 and $L'=1$ for $N=13$). For $N=13$, a second transition to an $L'=0$ state ($[1,1/2] \rightarrow [0,7/2]$) occurs at $\lambda \approx 9.0$. In most cases, the total spin S also increases, as expected for larger interaction strengths, but not in the increment of flipping one

spin at a time. These transitions could be detected by magnetic measurements. Many intermediate spin states with non-zero L are skipped, for example, $[2, 3/2]$ for $N=5$, $[1, 3/2]$ for $N=7$, and $[1, 5/2]$ for $N=9$. At large λ , the gain in exchange energy from having more than one half-filled shell with parallel-spin electrons outweighs the small level promotion energy, resulting in transitions to $L=0$ states (for example, $[0, 5/2]$ for $N=7$, $[0, 7/2]$ for $N=9$, and $[0, 7/2]$ for $N=13$). At $\lambda=10$, the ground states in Fig. 1 are either already an $L=0$ state, or close to becoming an $L=0$ state. The current numerical studies conclude that the path to Wigner crystallization is rather unique in circular quantum dots; the transitions to an $L=0$ state when the confinement gets weaker takes place in the intermediate density region already.

On the other hand, for some N values the classical ($\lambda \rightarrow \infty$) configuration of electrons is not consistent with $S=N/2$ and $L=0$. For $N \leq 8$, the classical minimum-energy configurations²³ consists of at most two shells, with $(k, N-k)$ electrons, where $k=0$ (one shell) for $N \leq 5$ and $k=1$ (two shells) for $N=6-8$. The electrons in the outer shell form a regular polyhedron. The z -axis is an $(N-k)$ -fold symmetry axis. A rotation of $2\pi/(N-k)$ about the z -axis is then equivalent to a cyclic permutation of the $(N-k)$ electrons, yielding

$$\hat{R} \left(\frac{2\pi}{N-k} \right) \Psi_L = \hat{P}(1, 2, \dots, N-k) \Psi_L, \quad (2)$$

where Ψ_L denotes the wave amplitude for the classical minimum-energy configuration. The rotation operator has an eigenvalue of $\exp[i2\pi L/(N-k)]$, while \hat{P} has an eigenvalue of $(-1)^{N-k-1}$, if Ψ_L is a fully polarized state. The condition that $\exp[i2\pi L/(N-k)] = (-1)^{N-k-1}$ for nonzero $\Psi_{L=0}$ is not satisfied when $N-k$ is even, i.e., for $N=2, 4$, and 7 . Hence the classical configuration of electrons is not consistent with $S=N/2$ and $L=0$. In these cases, at large λ the condition $L=0$ will take precedence over $S=N/2$ since the rotational energy goes as $\sim L^2/R^2$ (R is the size of an N -electron quantum dot in the Wigner state), whereas the exchange energy goes as $\exp(-C\sqrt{R})$.²⁴

The ground-state transitions that occur as λ is increased, shown in Fig. 1, can thus be understood as arising from a competition between four effects:

1. Lower-energy single-particle orbitals are filled before higher-energy ones (Aufbau principle).

2. High-spin states are favored compared to low-spin states. This not only determines the symmetry for a given configuration of electrons, but for sufficiently large λ it becomes energetically favorable to promote electrons from low-energy orbitals to higher-energy ones in order to increase S .

3. The rotational energy increases with L as $E_I \sim L^2/R^2$,¹¹ so states with low L are favored.

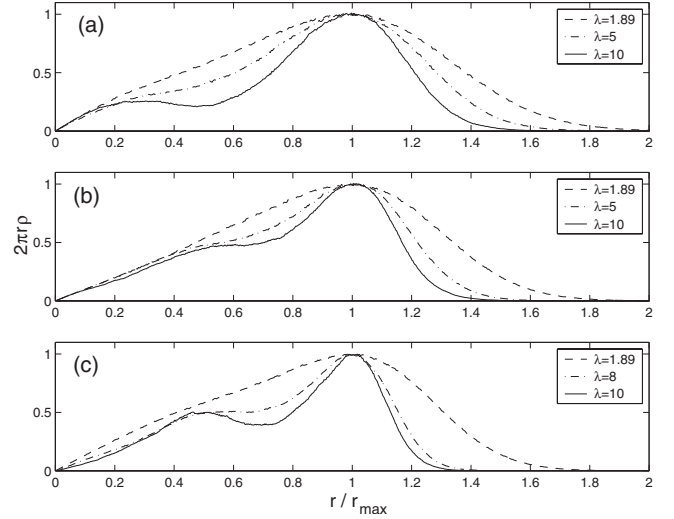


FIG. 2. Evolution of the charge density with increasing λ : (a) state $[0, \frac{1}{2}]$ for $N=7$; (b) state $[0, 0]$ for $N=10$; and (c) state $[1, \frac{1}{2}]$, for $N=13$. The radius r has been rescaled by r_{\max} , the location of the maximum of $2\pi r\rho(r)$.

4. Because of symmetry constraints, for some N values the localized Wigner state with $L=0$ does not become fully spin-polarized in circular quantum dots.

To examine the radial ordering of electrons as λ increases, we have calculated the charge density $\rho(r)$, which is independent of the angular coordinate for a circular quantum dot. Figure 2 shows charge densities for $N=7, 10$, and 13 in their ground states. The charge densities exhibit one peak when λ is small. A shoulder emerges in the vicinity of $r=0$ when $\lambda \geq 5$. The shoulder develops into a second peak as λ is further increased, showing a stronger radial ordering.

IV. CONCLUSION

In summary, using the diffusion quantum Monte Carlo method incorporating excited-state Slater determinants, we have obtained accurate ground-state energies for two-dimensional quantum dots containing $N=3-13$ electrons as a function of interaction strength. Our central finding is that as the density (effective interaction strength) decreases (increases), ground-state transitions take place to minimize angular momentum. While spin polarization also increases during these transitions, we show that a fully-spin-polarized Wigner molecule is only possible for some values of N based on quantum symmetry considerations.

ACKNOWLEDGMENTS

We thank Constantine Yannouleas and Uzi Landman for helpful discussions. This work is supported in part by the U.S. Department of Energy under Grant No. DE-FG02-97ER45632, the National Science Foundation under Grant No. DMR-02-05328, and the National Energy Research Scientific Computing Center (NERSC).

- ¹M. A. Kastner, *Rev. Mod. Phys.* **64**, 849 (1992); *Phys. Today* **46**(1), 24 (1993).
- ²R. C. Ashoori, *Nature (London)* **379**, 413 (1996); L. P. Kouwenhoven *et al.*, *Science* **278**, 1788 (1997).
- ³U. Meirav, M. A. Kastner, and S. J. Wind, *Phys. Rev. Lett.* **65**, 771 (1990).
- ⁴R. C. Ashoori, H. L. Stormer, J. S. Weiner, L. N. Pfeiffer, S. J. Pearton, K. W. Baldwin, and K. W. West, *Phys. Rev. Lett.* **68**, 3088 (1992).
- ⁵A. V. Filinov, M. Bonitz, and Yu. E. Lozovik, *Phys. Rev. Lett.* **86**, 3851 (2001).
- ⁶R. B. Laughlin, *Phys. Rev. Lett.* **50**, 1395 (1983).
- ⁷J. K. Jain, *Phys. Rev. Lett.* **63**, 199 (1989); J. K. Jain and T. Kawamura, *Europhys. Lett.* **29**, 321 (1995).
- ⁸M. Ferconi and G. Vignale, *Phys. Rev. B* **50**, 14722 (1994).
- ⁹H. M. Müller and S. E. Koonin, *Phys. Rev. B* **54**, 14532 (1996).
- ¹⁰C. Yannouleas and U. Landman, *Phys. Rev. Lett.* **82**, 5325 (1999); *Phys. Rev. B* **66**, 115315 (2002); **68**, 035325 (2003); **68**, 035326 (2003); **70**, 235319 (2004).
- ¹¹C. Yannouleas and U. Landman, *Phys. Rev. B* **69**, 113306 (2004).
- ¹²S. M. Reimann and M. Manninen, *Rev. Mod. Phys.* **74**, 1283 (2002) and references therein.
- ¹³R. Egger, W. Häusler, C. H. Mak, and H. Grabert, *Phys. Rev. Lett.* **82**, 3320 (1999); **83**, 462(E) (1999).
- ¹⁴S. M. Reimann, M. Koskinen, and M. Manninen, *Phys. Rev. B* **62**, 8108 (2000).
- ¹⁵F. Pederiva, C. J. Umrigar, and E. Lipparini, *Phys. Rev. B* **62**, 8120 (2000).
- ¹⁶B. Reusch and R. Egger, *Europhys. Lett.* **64**, 84 (2003).
- ¹⁷S. Weiss and R. Egger, *Phys. Rev. B* **72**, 245301 (2005).
- ¹⁸A. Ghosal, A. D. Güçlü, C. J. Umrigar, D. Ullmo, and H. U. Baranger, *Nat. Phys.* **2**, 336 (2006); *Phys. Rev. B* **76**, 085341 (2007).
- ¹⁹A. D. Güçlü, Amit Ghosal, C. J. Umrigar, and Harold U. Baranger, *Phys. Rev. B* **77**, 041301(R) (2008).
- ²⁰Real wave functions are obtained by combining the $+L$ and $-L$ eigenfunctions, which has the same energy expectation value as the true eigenfunction of H .
- ²¹When excited-state Slater determinants are included, we do not find a transition from state $[0, 1]$ to $[2, 1]$ at $\lambda \approx 8.0$ for $N=8$, as reported in Ref. 18.
- ²²S. A. Mikhailov, *Phys. Rev. B* **66**, 153313 (2002).
- ²³V. M. Bedanov and F. M. Peeters, *Phys. Rev. B* **49**, 2667 (1994).
- ²⁴B. Bernu, L. Candido, and D. M. Ceperley, *Phys. Rev. Lett.* **86**, 870 (2001).